ρ and K^* resonances on the lattice at nearly physical quark masses

Gunnar S. Bali,[1,2] Sara Collins,[1] Antonio Cox,[1] Gordon Donald,[1]
Meinulf Göckeler,[1] C. B. Lang,[3] and Andreas Schäfer[1]

(RQCD Collaboration)

[1]*Institute for Theoretical Physics, University of Regensburg, 93040 Regensburg, Germany*
[2]*Tata Institute of Fundamental Research, Homi Bhabha Road, Mumbai 400005, India*
[3]*Institute of Physics, University of Graz, A-8010 Graz, Austria*
(Dated: December 31, 2015)

Working with a pion mass $m_\pi \approx 150$ MeV, we study $\pi\pi$ and $K\pi$ scattering using two flavours of non-perturbatively improved Wilson fermions at a lattice spacing $a \approx 0.071$ fm. Employing two lattice volumes with linear spatial extents of $N_s = 48$ and $N_s = 64$ points and moving frames, we extract the phase shifts for p-wave $\pi\pi$ and $K\pi$ scattering near the ρ and K^* resonances. Comparing our results to those of previous lattice studies, that used pion masses ranging from about 200 MeV up to 470 MeV, we find that the coupling $g_{\rho\pi\pi}$ appears to be remarkably constant as a function of m_π.

I. INTRODUCTION

Lattice QCD calculations are particularly well suited for hadrons which are stable under the strong interaction and their properties can be determined by studying correlation functions at large Euclidean time separations. However, almost all known hadrons are unstable resonances, which complicates the situation. The ρ meson, one of the simplest resonances in QCD, couples to a pair of pions with total isospin $I = 1$. In a finite lattice volume of linear spatial size $L = N_s a$, the allowed momenta of the pion pair are quantized. Neglecting $\pi\pi$ interactions, the lowest lying $\pi\pi$ state with the same spin $J = 1$ as the ρ has the energy

$$E_{\pi\pi}^{\text{free}} = 2\sqrt{m_\pi^2 + \left(\frac{2\pi}{L}\right)^2}. \qquad (1)$$

The ρ can only be treated as a stable particle if its mass is sufficiently smaller than this $\pi\pi$ centre of momentum frame energy $E_{\pi\pi}^{\text{free}}$. This is possible if the pion is heavy or the lattice size is small. For the values of m_π and L that are now accessible in lattice simulations this is not the case anymore.

The formalism for dealing with resonances in lattice QCD simulations of two-particle scattering systems has been developed first with equal masses and in systems at rest [1, 2] and later extended to various moving frames and unequal masses [3–10]. In $\pi\pi$ scattering, the ρ appears as an increase of the scattering phase shift from zero to π as the centre of momentum frame energy, E_{cm}, is varied from below to above the resonant mass value m_ρ. The dependence of the $\ell = 1$ angular momentum partial wave shift δ on E_{cm} gives detailed information about the nature of the resonance. The position of the real part of the pole, i.e. the resonant mass, can be extracted at the value $\delta = \pi/2$.

Due to the computational cost, previous calculations of the resonance parameters were restricted to unphysically large pion masses (most even employed pion masses with $E_{\pi\pi}^{\text{free}} > m_\rho$), but the expected phase shift behaviour was still observed [6, 11–19]. Algorithmic advances and increases in compute power now enable us to pursue the first scattering study at a close to physical pion mass $m_\pi \approx 150$ MeV.

The strange-light analogue of the light-light ρ meson is the K^*. Also its phase shift has been studied previously in lattice calculations at unphysically large pion masses [20–23]. There are similarities between $\pi\pi$ and $K\pi$ scattering not only in terms of the formalism but also in terms of constructing and computing the necessary correlation functions, which means we can incorporate the K^* resonance into our study, with limited computational overhead.

From experiment, the ρ has a mass of around 775 MeV and a decay width $\Gamma_\rho \approx 148$ MeV while the K^* mass and width are approximately 896 MeV and 47 MeV [26]. The decays are almost exclusively to $\pi\pi$ and $K\pi$, respectively. In our study of the ρ resonance we neglect couplings to three- and four-pion states. Our calculation (and all other $\pi\pi$ scattering calculations to-date) is performed with isospin symmetry in place, therefore 3π final states are excluded. Isospin symmetry tremendously simplifies the computation for the $I = 1$ ρ and the $I = 1/2$ K^* channels we consider here as there are no disconnected quark-line contractions. As we will see, at our pion mass and for the kinematics we implement, only one of our data points could be sensitive to 4π final states. Also, considering the available phase space and Okubo-Zweig-Iizuka suppression, neglecting these multiparticle final states should a very good approximation. This argument is supported by experimental evidence, indeed suggesting a virtually undetectable coupling of the ρ meson to 4π states [27]. Comparing measurements of the branching fractions of $\rho \to 4\pi$ and the (isospin breaking) $\rho \to 3\pi$ decay [27, 28] shows that they are of similar (small) sizes. For a neutral ρ meson, the decay width to $\pi^+\pi^-\pi^0$ is 15(7) keV. Combining the widths to $\pi^+\pi^-\pi^0\pi^0$ and $\pi^+\pi^-\pi^+\pi^-$ gives 5(2) keV. This is indeed negligible, relative to the total width of 148 MeV.

TABLE I. Details of the lattice configurations: volume, coupling, lattice spacing (determined in Ref. [24]), light and strange quark mass parameters κ_ℓ and κ_s, (finite volume) pion mass, kaon mass, the linear spatial size in units of the infinite volume pion mass Lm_π^∞ [25], the unit momentum $2\pi/L$ and the number of configurations $N_{\rm cfg}$ analysed. The errors given for m_π and m_K are statistical only and do not include the 3% scale setting uncertainty [24].

$N_s^3 \times N_t$	β	a^{-1}	κ_ℓ	κ_s	m_π	m_K	Lm_π^∞	$2\pi/L$	$N_{\rm cfg}$
$48^3 \times 64$	5.29	2.76(8) GeV	0.13640	0.135574	160(2) MeV	500(1) MeV	2.61	361 MeV	888
$64^3 \times 64$	5.29	2.76(8) GeV	0.13640	0.135574	150(1) MeV	497(1) MeV	3.48	271 MeV	671

For decays of a charged ρ into four pions only an upper limit exists.

In the cases of $\pi\pi$ and $K\pi$ scattering, respectively, in principle there could also be interference with $K\bar{K}$ and $K\eta$; $2m_K \approx 985\,{\rm MeV}$, $m_K + m_\eta \approx 1040\,{\rm MeV}$. However, both values are well above the region we are interested in, in particular considering p-wave decay in a finite volume. For heavier than physical pions, these thresholds are closer. This situation was studied at $m_\pi \approx 236$ MeV in Ref. [18] for the ρ resonance and at $m_\pi \approx 391$ MeV in Ref. [23] for the K^*. Indeed, even at these large pion masses, the impact was found to be negligible. Finally, we also ignore $K^* \to K\pi\pi$, noting that the upper limit reads $\Gamma(K^* \to K\pi\pi) \approx 35\,{\rm keV}$ [29]; the vast majority of experimentally observed decays to $K\pi\pi$ final states appear to be related to heavier resonances [30].

Our method to generate the necessary correlation functions has been employed in previous calculations [6, 11, 14]. Nevertheless, we provide a brief description of the construction of correlators, along with details on the lattices and kinematics used in Section II. The results are presented and discussed in Section III, before we conclude in Section IV.

II. LATTICE CALCULATION

We aim to extract the resonance parameters (mass and width) of the ρ and K^* from their appearances in $\pi\pi$ and $K\pi$ p-wave scattering, respectively. To do so, we will determine the spectra of interacting two-particle QCD states in finite volumes. Using these energy levels, along with known relations, allows us to extract the scattering phase shift, from whose dependence on the energy E_{cm} in the rest frame of the ρ (or the K^*) the resonance parameters can be found.

A. Discussion of the lattice parameters

We employ lattice configurations with a lattice spacing $a \approx 0.071\,{\rm fm}$ and time extent $N_t a = 64a \approx 4.6\,{\rm fm}$, generated by RQCD ($64^3$ spatial volume) and RQCD/QCDSF (48^3 volume) with $N_f = 2$ flavours of degenerate non-perturbatively improved Wilson sea quarks with a pion mass of about 150 MeV (ensembles VIII and VII of

Ref. [31]). On the larger volume every second trajectory and on the smaller volume every fifth trajectory is analysed. Discretization errors are of $\mathcal{O}(a^2)$. We expect these to be small for the light hadron masses considered at our lattice scale $a^{-1} = 2.76(8)\,{\rm GeV}$ [24]. The lattice parameters are given in Table I. More detail can be found in Refs. [25, 31]. Following Ref. [32], we check the strange quark mass tuning by computing $\sqrt{2m_K^2 - m_\pi^2} = 686.5(1.1)\,{\rm MeV}$ on the $N_s = 64$ ensemble, assuming $a^{-1} = 2.76\,{\rm GeV}$. We find perfect agreement with the "experimental" value of 686.9 MeV.

The choice of our ensembles is motivated by the proximity of the pion mass to its experimental value. In the $\rho \to \pi\pi$ channel the pions must have relative angular momentum. For a system at rest this is only possible if their individual momenta are non-zero. This gives the threshold Eq. (1), where $m_\rho > E_{cm}^{\rm free} > 2m_\pi$, for the ρ to become unstable in a finite volume. On our lattice configurations, this threshold lies at 782 MeV (within the experimental ρ resonance width) for $N_s = 48$ and at 619 MeV (beneath the resonance) for $N_s = 64$. Note that in moving frames the effective thresholds can be lower.

The combination Lm_π is the relevant quantity controlling finite size effects. This combination obviously decreases with m_π and it is expensive to enlarge the linear box size L to fully compensate for this. Our lattice volumes have $Lm_\pi < 4$, due to limited computer resources. However, there are clear advantages employing small volumes to resolve broad resonances like the ρ: At large L the spectrum of two-particle states becomes dense, complicating the extraction of the relevant energy levels and increasing the demand on the precision of their determination.

Terms which are exponentially suppressed in Lm_π are neglected in the Lüscher phase shift method [1]. One such effect is the difference between the pion mass $m_\pi \approx 160\,{\rm MeV}$ on the small volume and its infinite volume value $m_\pi^\infty \approx 149.5\,{\rm MeV}$ [31], which goes beyond this formalism. Note that $Lm_\pi^\infty \approx 2.6$ for our smaller volume and $e^{-2.6} \approx 0.074$ may not necessarily be considered a small number. Fortunately, it has been demonstrated, at least in some models, e.g., in the inverse amplitude and the N/D_A models, that for $I = 1$ p-wave $\pi\pi$ scattering the corrections to the Lüscher formula may be negligible as long as $Lm_\pi > 2$ [33]. We note that towards small pion masses the ρ resonance broadens, allowing us to extract

non-trivial phase shifts for a wider range of energies than had been possible in previous simulations at unphysically large pion masses. This allows us to collect several data points within the region relevant to constrain the resonance parameters.

An issue that arises for pions which are sufficiently close to their physical mass is the opening of the four-pion threshold as, in nature, $m_\rho > 4m_\pi$. In analogy to our discussion of two-particle thresholds, we can determine where the four-particle thresholds will lie for the lattice configurations we use. When the ρ meson is at rest at least two of the pions need to carry non-zero momenta. In this case, a decay to four pions requires 918 MeV on our larger lattice size and 1081 MeV on the smaller one, both of which lie well above the resonance region.

Again, for moving frames, these limits can be lower. We encounter the worst case for the total momentum $\mathbf{P} = (0,0,1)(2\pi/L)$ on $L = 64a$, where the four-pion threshold lies around $E_{cm} = 710$ MeV. Fortunately, as we discussed in the introduction, the ρ and K^* resonances are entirely dominated by p-wave decays into $\pi\pi$ and $K\pi$ final states; even in experiment other channels are hardly detectable at all. Finally, we remark that dealing with decays to more than two particles in lattice QCD is an open problem. While there has been recent theoretical progress addressing three-particle final states [34–36], for now it is not even known how to analyse four-pion states.

B. Generation of the correlators

In order to treat the ρ as a resonance in $\pi\pi$ scattering, we employ a basis of interpolators which explicitly couple to one- and two-particle states. The interpolators used for each kinematic setting all share the same quantum numbers and symmetries. In the case of $\pi\pi$ scattering, we are interested in the $I = 1$, $J^P = 1^-$ channel in which the ρ appears. The $\pi\pi$ interpolators read

$$\pi(\mathbf{p_1})\pi(\mathbf{p_2}) = \frac{1}{\sqrt{2}}\left[\pi^+(\mathbf{p_1})\pi^-(\mathbf{p_2}) - \pi^-(\mathbf{p_1})\pi^+(\mathbf{p_2})\right] ,$$
(2)

where $\pi = \bar{\psi}\gamma_5\psi$ and the one-particle vector interpolator has the momentum $\mathbf{P} = \mathbf{p_1} + \mathbf{p_2}$. For this we use three structures in our basis: $\bar{\psi}\gamma_j\psi$, $\bar{\psi}\gamma_j\gamma_t\psi$ and $\bar{\psi}\nabla_j\psi$.

We apply Wuppertal quark smearing [37], where the field, $\phi_x^{(n)}$, at site x after n smearing iterations is

$$\phi_x^{(n)} = \frac{1}{1+6\delta}\left(\phi_x^{(n-1)} + \delta\sum_{j=\pm1}^{\pm3} U_{x,j}\phi_{x+a\hat{\jmath}}^{(n-1)}\right) . \quad (3)$$

We set $\delta = 0.25$ and employ three levels of quark smearing, using 50, 100 or 150 iterations. $U_{x,\mu}$ is a (smeared) gauge link connecting x with $x+a\hat{\mu}$ and $U_{x,-\mu} = U_{x-a\hat{\mu},\mu}^\dagger$. For the pseudoscalar meson operators, we choose the narrowest smearing width. We use all three smearing levels for $\bar{\psi}\gamma_j\psi$ and $\bar{\psi}\gamma_j\gamma_t\psi$ and only the narrowest for
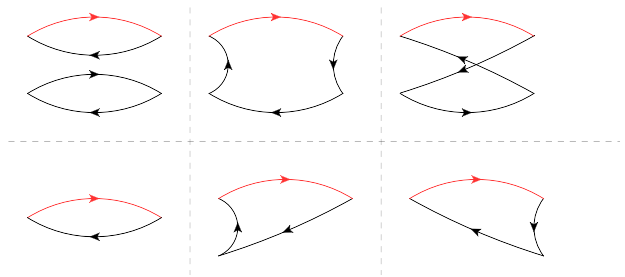

FIG. 1. Diagrams showing the quark contractions for the entries of our correlation matrices for $\pi\pi$ and $K\pi$ scattering. The red propagator denotes a strange quark for $K\pi$ and a light one for $\pi\pi$, while the black propagators are for light quarks in both cases. The top row shows contractions for $2 \to 2$ particle correlators. The right-most diagram does not appear for $I = 1$ $\pi\pi$ scattering, but is required for our $K\pi$ scattering calculation. The second row contains $1 \to 1$, $2 \to 1$ and $1 \to 2$ entries, respectively, where the $1 \to 2$ element is the conjugate complex of $2 \to 1$.

$\bar{\psi}\nabla_j\psi$, so we have one two-particle interpolator and a total of seven one-particle interpolators. We employ spatial APE smearing for the gauge links [38] that appear within Eq. (3) above:

$$U_{x,i}^{(n)} = P_{\mathrm{SU}(3)}\left(\alpha\, U_{x,i}^{(n-1)} + \sum_{|j|\neq i} U_{x,j}^{(n-1)} U_{x+a\hat{\jmath},i}^{(n-1)} U_{x+a\hat{\imath},j}^{(n-1)\dagger}\right)$$
(4)

with $i \in \{1,2,3\}, j \in \{\pm1,\pm2,\pm3\}$. $P_{\mathrm{SU}(3)}$ denotes a projection into the SU(3) group. We use $\alpha = 2.5$ and 25 iterations.

In $K\pi$ scattering, the K^* resonance is in the $I = 1/2$ channel, so we use

$$\pi(\mathbf{p_1})K(\mathbf{p_2}) = \sqrt{\frac{2}{3}}\pi^+(\mathbf{p_1})K^-(\mathbf{p_2}) - \sqrt{\frac{1}{3}}\pi^0(\mathbf{p_1})K^0(\mathbf{p_2})$$
(5)

as the two-particle interpolator. The one-particle interpolators are the same as for the ρ resonance, replacing a light quark by the strange. From these interpolators we calculate a matrix of correlation functions, whose entries are depicted in Figure 1.

By using the two volumes and a number of moving frames, we are able to access several points within the regions of interest around the expected positions of the ρ and K^* resonances. The kinematic points we use are given in Table II, where

$$\mathbf{K} = \frac{L}{2\pi}\mathbf{P} \quad (6)$$

denotes an integer-valued lattice momentum vector. The choice of momenta and representations is based on the requirement that the non-interacting two-particle states lie within or close to the expected resonance widths. To allow reuse of the generated propagators, we restrict ourselves to $\mathbf{k_1} = \mathbf{p_1}L/(2\pi) = (1,0,0)$. For each total

TABLE II. The interpolators we use in different moving frames. For each frame, we note the little group and irreducible representations (irrep) we employ and the one- and two-particle interpolators that belong to them. **K** denotes the integer valued total momentum vector (used for the one-particle interpolator) and the arguments of the pseudoscalar interpolators are $\mathbf{k}_j = \mathbf{p}_j L/(2\pi)$.

$\pi\pi$					
N_s	**K**	(Little) group	Irrep	$\mathcal{O}_{\pi\pi}$	$\mathcal{O}_\rho$
48	$(0,0,0)$	O_h	T_1	$\pi(1,0,0)\pi(-1,0,0)$	ρ_x
48	$(0,0,1)$	C_{4v}	E	$\pi(1,0,0)\pi(-1,0,1) - \pi(-1,0,0)\pi(1,0,1)$	ρ_x
48	$(0,1,1)$	C_{2v}	A_1	$\pi(1,0,0)\pi(-1,1,1) + \pi(-1,0,0)\pi(1,1,1)$	$\rho_y + \rho_z$
48	$(0,1,1)$	C_{2v}	B_1	$\pi(1,0,0)\pi(-1,1,1) - \pi(-1,0,0)\pi(1,1,1)$	ρ_x
64	$(0,0,1)$	C_{4v}	E	$\pi(1,0,0)\pi(-1,0,1) - \pi(-1,0,0)\pi(1,0,1)$	ρ_x
64	$(0,1,1)$	C_{2v}	A_1	$\pi(1,0,0)\pi(-1,1,1) + \pi(-1,0,0)\pi(1,1,1)$	$\rho_y + \rho_z$
64	$(0,1,1)$	C_{2v}	B_1	$\pi(1,0,0)\pi(-1,1,1) - \pi(-1,0,0)\pi(1,1,1)$	ρ_x
$K\pi$					
N_s	**K**	(Little) group	Irrep	$\mathcal{O}_{K\pi}$	$\mathcal{O}_{K^*}$
48	$(1,1,0)$	C_{2v}	B_2	$\pi(1,0,0)K(0,1,0)$	$K_x^* - K_y^*$
64	$(0,0,0)$	O_h	T_1	$\pi(1,0,0)K(-1,0,0)$	K_x^*
64	$(0,0,1)$	C_{4v}	E	$\pi(1,0,0)K(-1,0,1) - \pi(-1,0,0)K(1,0,1)$	K_x^*
64	$(0,1,1)$	C_{2v}	A_1	$\pi(1,0,0)K(-1,1,1) + \pi(-1,0,0)K(1,1,1)$	$K_y^* + K_z^*$
64	$(0,1,1)$	C_{2v}	B_1	$\pi(1,0,0)K(-1,1,1) - \pi(-1,0,0)K(1,1,1)$	K_x^*

momentum **P**, we have to construct interpolators which transform according to a definite irreducible representation (irrep) of the little group of allowed cubic rotations once a Lorentz boost has been applied. We construct the interpolators using the information about the little groups given in Ref. [10]. The irreps we work with and the (one- and two-particle) interpolators that transform according to each representation are also listed in Table II. We use Schoenflies notation (see, for example, Ref. [39]) for the names of the groups and irreps.

The necessary quark line contractions are depicted in Figure 1, where the first row includes two-particle to two-particle transitions and the second row one- to one- as well as two- to one-hadron transitions. We use stochastic $\mathbb{Z}_2 + i\mathbb{Z}_2$ wall sources at one time slice for each spin component and, for the contractions involving the two-particle interpolators, sequential inversions to generate all the contributing diagrams, following Refs. [11, 14]. To compute the top left contraction of Figure 1, it is necessary to use two stochastic sources per configuration. We use this minimum number of estimates per configuration as the gauge noise dominates. We further reduce the computational cost by fixing $\mathbf{k}_1$ to $(1,0,0)$. Even with this restriction, we can obtain several interesting levels around the expected positions of the ρ and K^* resonances. Moreover, we only compute the full $\pi\pi \to \pi\pi$ correlator from $t = 6a$ to $t = 17a$, where we anticipate that on one hand the signal is only moderately polluted by excited state contributions and on the other hand statistical errors are still tolerable. We are also able to "recycle" many propagators in both $\pi\pi$ and $K\pi$ scattering.

Adding this up, in our implementation the total number of solves required on each configuration is

$$N_{\text{vec}} \left[N_{\text{smear}} + N_{p_1}(1 + 18N_{p_2} + 3N_{\text{times}}) \right], \quad (7)$$

where $N_{\text{vec}} = 8$ is the number of noise sources used (four spin components times two different vectors), $N_{\text{smear}} = 4$ is the number of one-particle smearing levels (three plus one derivative source, see below), $N_{p_1} = 1$ and N_{p_2} (see Table II) are the numbers of momenta calculated and $N_{\text{times}} = 12$ ($t = 6a$ up to $t = 17a$) is the number of time slices for which the box diagrams shown in the top middle and top right of Figure 1 are calculated. For the $N_s = 48$ and $N_s = 64$ lattices, evaluating the full eight by eight matrices of correlators for each moving frame amounts to inverting the strange quark Wilson matrix 80 and 120 times, respectively, and the light quark matrix 824 and 808 times. Note that the number of solves required to compute a "traditional" point-to-all propagator is twelve, i.e. the present scattering computation is by a factor of about 40 more expensive than a conventional determination of the spectrum of stable light hadrons for one quark smearing level (twelve strange and twelve light quark inversions on each volume).

The momenta injected are not indicated in Figure 1 and the correlator is the sum of all allowed momentum projections; some irreps require a combination of two related pairs of momenta and, in $\pi\pi$ scattering, we can interchange the momenta $\mathbf{p}_1$ and $\mathbf{p}_2$ carried by each pion at the sink. Similarly, we ensure that the one-particle to one-particle correlators — depicted in the lower left of the figure — transform according to the irreps given in Table II, by taking the corresponding combinations of vector meson polarizations. The contractions for $\pi\pi \to \rho$ and $\rho \to \pi\pi$ are complex conjugates and it is computationally cheaper to only calculate one of them. (We do this for $\pi\pi \to \rho$.) For the remaining correlation matrix elements with $i \neq j$ (one- to one-particle), we average over C_{ij} and C_{ji}^*.

C. Extraction of energy levels and phase shifts

For each kinematic situation, we construct an eight times eight matrix of correlators for our basis of interpolators in the way described above. The element of this matrix for a source interpolator $\mathcal{O}_j$ and a sink interpolator $\mathcal{O}_i$ is given as

$$C_{ij}(t) = \langle 0|\hat{\mathcal{O}}_i(t)\hat{\mathcal{O}}_j^\dagger(0)|0\rangle \,. \qquad (8)$$

The spectral decomposition can be written as

$$C_{ij}(t) = \sum_\alpha \frac{Z_\alpha^i Z_\alpha^{j*}}{2E^\alpha} e^{-E^\alpha t} \,, \qquad (9)$$

where $Z_\alpha^i = \langle 0|\hat{\mathcal{O}}_i|\alpha\rangle$ is the overlap factor of the state created by the operator $\hat{\mathcal{O}}_i^\dagger$ with the physical state $|\alpha\rangle$ of energy E^α. We extract the energy levels E^α by solving the generalized eigenvalue problem [40–42]

$$C(t)u^\alpha(t) = \lambda^\alpha(t_0,t)C(t_0)u^\alpha(t) \,, \qquad (10)$$

where the energy levels can be obtained from the dependence $\lambda^\alpha(t_0,t) \sim e^{-E^\alpha(t-t_0)}$ at large times.

The energies we extract are in the lab frame, so we denote these as E_L. The phase shift, however, is extracted in the centre of momentum frame, i.e. in the rest frame of the $\pi\pi$- or πK-system. It is straightforward to convert the lab frame energies E_L into the corresponding centre of momentum frame energies E_{cm}.

The lab frame energy of the two-meson state is given as

$$E_L = \sqrt{\mathbf{p}_1^2 + m_1^2} + \sqrt{\mathbf{p}_2^2 + m_2^2} \,, \qquad (11)$$

where the m_i are the pion (or kaon) masses and the $\mathbf{p}_i$ their momenta. In the absence of interactions the $\mathbf{p}_i^2$ are integer multiples of $(2\pi/L)^2$. The invariant squared energy in the centre of momentum frame is

$$E_{cm}^2 = E_L^2 - \mathbf{P}^2 \,, \qquad (12)$$

where $\mathbf{P}$ is the total momentum of the $\pi\pi$ (or the $K\pi$) system. The square of the momentum of each of the pseudoscalars in the centre of momentum frame is given by

$$p_{cm}^2 = \frac{\left(E_{cm}^2 - (m_1 + m_2)^2\right)\left(E_{cm}^2 - (m_1 - m_2)^2\right)}{4E_{cm}^2} \,. \qquad (13)$$

The phase shift is extracted, comparing the centre of momentum frame spectrum to the energy levels allowed by the residual cubic symmetry (little group) that corresponds to the boost applied. For each irrep, this involves an expression in terms of generalized zeta functions, derived in Refs. [9, 10]. For the numerical calculation of these functions, we use the representation given in Ref. [10].

The generalized zeta function is a function of the real-valued variable $q = p_{cm}L/(2\pi)$:

$$Z_{\ell m}(q^2) = \sum_{\mathbf{z}} \frac{\mathcal{Y}_{\ell m}(\mathbf{z})}{\mathbf{z}^2 - q^2} \,, \qquad (14)$$

where $\mathcal{Y}_{\ell m}(\mathbf{z}) = |\mathbf{z}|^\ell Y_{\ell m}(\mathbf{e}_z)$ with $\mathbf{e}_z = \mathbf{z}/|\mathbf{z}|$ and $Y_{\ell m}$ are the usual spherical harmonics. The sum is over $\mathbf{z}$, the allowed momentum vectors in the boosted frame, see, e.g., Ref. [10].

For each irrep we have to consider mixing between different continuum partial waves. The relevant determinants from which the phase shifts can be extracted are listed in Ref. [10]. Here, we neglect $\ell \neq 1$, which should be a good approximation since in all but the $\mathbf{K} = (0,1,1)$ A_1 irrep, there is no mixing of $\ell = 0$ into $\ell = 1$.

Subsequently, we parameterize the phase shift as a function of the centre of momentum frame energy using a Breit-Wigner ansatz:

$$\tan\delta = \frac{g^2}{6\pi} \frac{p_{cm}^3}{E_{cm}(m_R^2 - E_{cm}^2)} \,. \qquad (15)$$

From this parametrization, we can extract the mass of the resonance m_R and its width can be found from the coupling g as

$$\Gamma = \frac{g^2}{6\pi} \frac{p_R^3}{m_R^2} \,, \qquad (16)$$

where p_R is the momentum carried by each particle in the centre of momentum frame at $\delta = \pi/2$, i.e. p_R is given by p_{cm} of Eq. (13) for $E_{cm} = m_R$.

III. RESULTS

A. Determination of the energy levels

Following the generalized eigenvalue procedure detailed in Section II C above, we separately analyse the eight by eight matrices that cross-correlate states created by one- and two-particle interpolators for the seven $\pi\pi$ and five $K\pi$ channels listed in Table II, and obtain the respective ground and first excited state energies. We are able to resolve these energies most easily using sub-matrices of correlators containing only three interpolators — one of which always is the two-particle interpolator $\mathcal{O}_{\pi\pi}$ or $\mathcal{O}_{K\pi}$ of Table II. The single-particle interpolators used in the final analysis are only of the type $\bar{\psi}\gamma_j\psi$. However, we have checked these results against employing other sub-matrices and found consistency of the effective masses, but no improvement. The results turned out very similar but often noisier when replacing one $\bar{\psi}\gamma_j\psi$ interpolator by $\bar{\psi}\gamma_j\gamma_t\psi$ while the $\bar{\psi}\nabla_j\psi$ interpolator increased the statistical errors very significantly, in particular for states with total momentum $\mathbf{K} = (0,1,1)$.

To save computer time we only evaluated the box diagrams in the top middle and top right of Figure 1 for
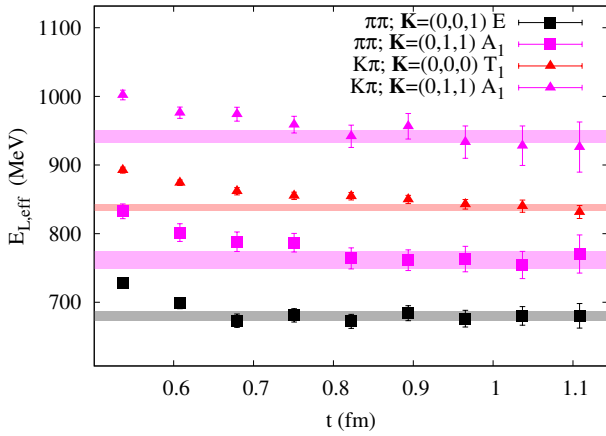
FIG. 2. Effective masses for some $\pi\pi$ and $K\pi$ channels. The error bands correspond to the fit results.

$17a \geq t \geq 6a$. The top left diagram contains two traces and naively increases like L^6 while the quark-line connected box diagrams have magnitudes $\propto L^3$. Due to this relative suppression, these can only become important at times of at least a similar magnitude as the inverse energy gap between $I = 2$ and $I = 1$ $\pi\pi$ (or $I = 3/2$ and $I = 1/2$ $K\pi$) states and probably their contribution to the $\pi\pi \to \pi\pi$ and $K\pi \to K\pi$ entries can be neglected at $t < 6a$. Nevertheless, to be on the safe side, in our generalized eigenvector analysis we set $t_0 = 6a \approx 0.43$ fm.

We show effective masses

$$E_{L,\text{eff}}^{\alpha}(t + a/2) = \frac{1}{a} \ln \frac{\lambda^{\alpha}(t_0 = 6a, t)}{\lambda^{\alpha}(t_0 = 6a, t + a)} \qquad (17)$$

for some of our $\pi\pi$ and $K\pi$ eigenvalues, see Eq. (10), in Figure 2, for the region $t > t_0 + a$. To enable better comparison to other studies, we display the data in physical units. The effective masses are typically consistent with plateaus between $t = 10a \approx 0.71$ fm and $17a \approx 1.22$ fm, which is our most frequent fit range, although there are differences between the channels. The $K\pi$ T_1 channel shown in the figure is an extreme example, where the fit range starts at $t = 14a \approx 1$ fm.

Of particular interest are the $\mathbf{K} = (0, 1, 1)$ A_1 channels since the non-interacting ground states in this irrep correspond to a momentum distribution among the two pseudoscalar mesons that differs from the one used in constructing our two-particle interpolators ($\mathbf{k}_1 = (1, 0, 0)$ and $\mathbf{k}_2 = \mathbf{K} - \mathbf{k}_1 = (-1, 1, 1)$ instead of the lower lying combination $\mathbf{k}_1 = \mathbf{0}$ and $\mathbf{k}_2 = \mathbf{K} = (0, 1, 1)$). In principle, these correlation functions could decay towards these lower lying states. However, we find no indication for this in our data, see Figure 2, and conclude that our interpolators effectively decouple from these energy levels.

The resulting lab frame energy levels E_L are shown in Figure 3 both for the $\pi\pi$ and $K\pi$ channels. The scale is set using $a^{-1} = 2.76$ GeV, ignoring the 3% overall scale uncertainty for the moment being. The statistical errors are obtained using the jackknife procedure. Only two

$\pi\pi$ levels are above the four-pion threshold (the excited states in the $\mathbf{K} = (0, 0, 1)$ E irrep), one of which will be disregarded in any case in the phase shift analysis below.

In the figure, we also show the energies of the non-interacting two-particle states. The solid horizontal lines are the non-interacting levels corresponding to the two-particle interpolators explicitly included in our basis (given in Table II), while the dashed lines correspond to other distributions of the momentum among the non-interacting pseudoscalar mesons. As we have not included interpolators that explicitly resemble these momentum configurations, we cannot rely on our extracted energy levels to be sensitive to their presence and ignore these non-interacting levels in our phase shift analysis. As already discussed above, in the A_1 case the non-interacting ground states are lower in energy than the levels that correspond to the momentum distribution we have implemented (solid lines). Nevertheless, we see no evidence of any coupling of the interpolators within our basis to these states, see Figure 2. Note that for the $N_s = 64$ $\pi\pi$ channel this level lies at 561 MeV, below the energy region shown in Figure 3.

Levels that are irrelevant, due to large statistical errors for the resulting phase shifts, will be excluded from our Breit-Wigner analysis. These levels are depicted as crosses in Figure 3. We remind the reader that the deviations of the measured energy levels shown in the figure from the non-interacting two-particle levels (solid lines) are due to the ρ and K^* resonances and encode the resonance parameters.

B. Phase shift and resonance parameters

The centre of momentum frame energies E_{cm} and phase shifts $\delta(E_{cm})$ can both be extracted from measured lab frame energy levels E_L in a given irrep, see Section II C, where we assume $m_\pi = 149.5$ MeV, in spite of the fact that the measured pion mass on the small volume is by 10 MeV larger. This will be addressed in Section III C below.

We plot $\delta(E_{cm})$ in Figure 4, using the same colour and symbol scheme as in Figure 3. In our determination of the phase shift, we assume that one value of ℓ ($\ell = 1$) dominates, such that there is a one to one correspondence between the extracted energy levels and the points in the phase shift curves. For clarity we omit all data points from the figure with errors on the phase shift in excess of $\pi/5$ (marked as crosses in Figure 3). These have little statistical impact and are therefore excluded from our Breit-Wigner analysis.

The $\pi\pi$ and $K\pi$ phase shifts are each fitted to the Breit-Wigner resonance form given in Eq. (15). Our fit to the $\pi\pi$ phase shift results in $\chi^2/\text{d.o.f} = 8.9/7$ and for the $K\pi$ phase shift we obtain $\chi^2/\text{d.o.f.} = 19.2/7$. These fits are included in Figure 4 (the grey hashed band for $\pi\pi$ scattering and the solid orange one for $K\pi$ scattering). In the $\pi\pi$ case the dashed data point of the figure
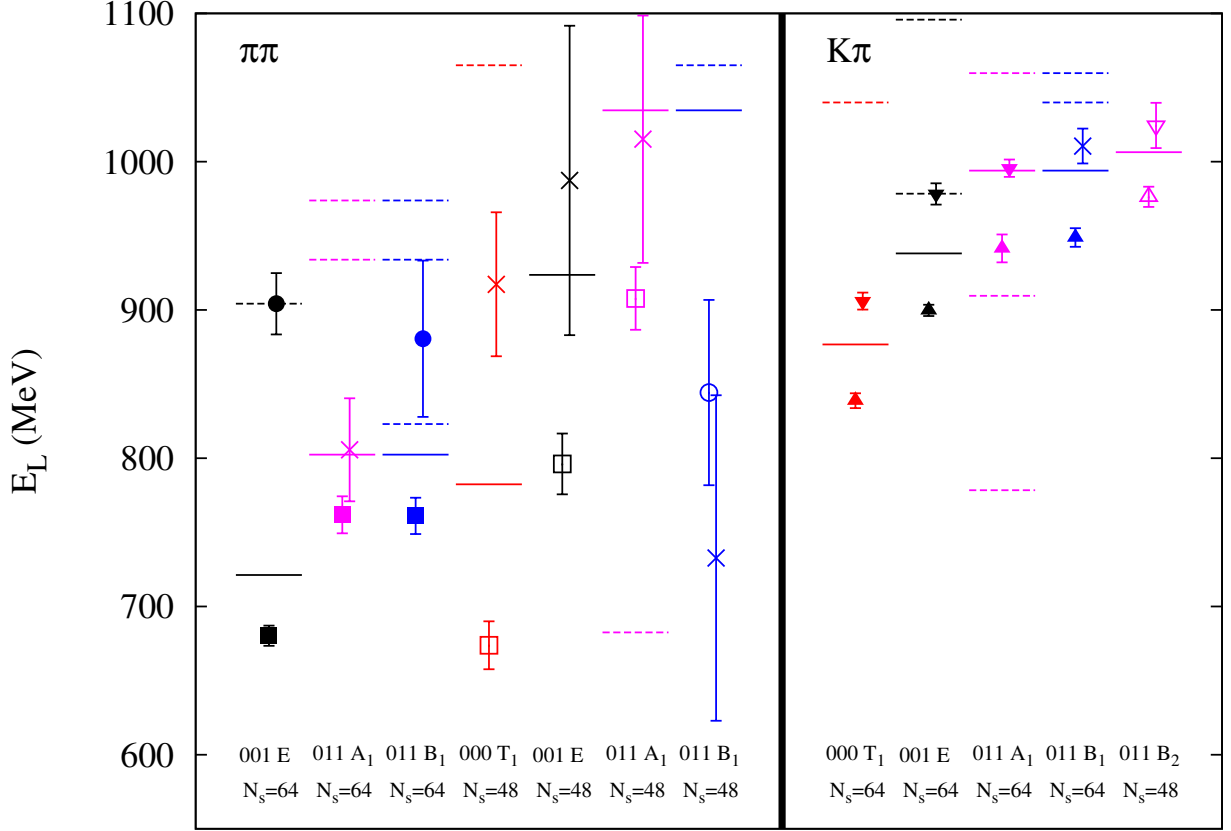
FIG. 3. Energy levels of the $\rho|\pi\pi$ (left) and $K^*|K\pi$ (right) systems in finite boxes of linear sizes $N_s a = 48a \approx 2.6/m_\pi^\infty \approx 3.4\,\mathrm{fm}$ and $N_s a = 64a \approx 3.5/m_\pi^\infty \approx 4.6\,\mathrm{fm}$ for different lattice momenta and representations in the laboratory frame. Horizontal lines correspond to the energy levels of a non-interacting two-particle system. Squares and upward pointing triangles indicate ground states, circles and downward pointing triangles first excited states. Open symbols correspond to the smaller volume and full symbols to the larger volume. Crosses are for levels that are not used in our subsequent phase shift analysis. Note that for $\pi\pi$ scattering the excited states in both $\mathbf{K} = (0,0,1)$ E channels are above the respective non-interacting 4π thresholds (not shown).
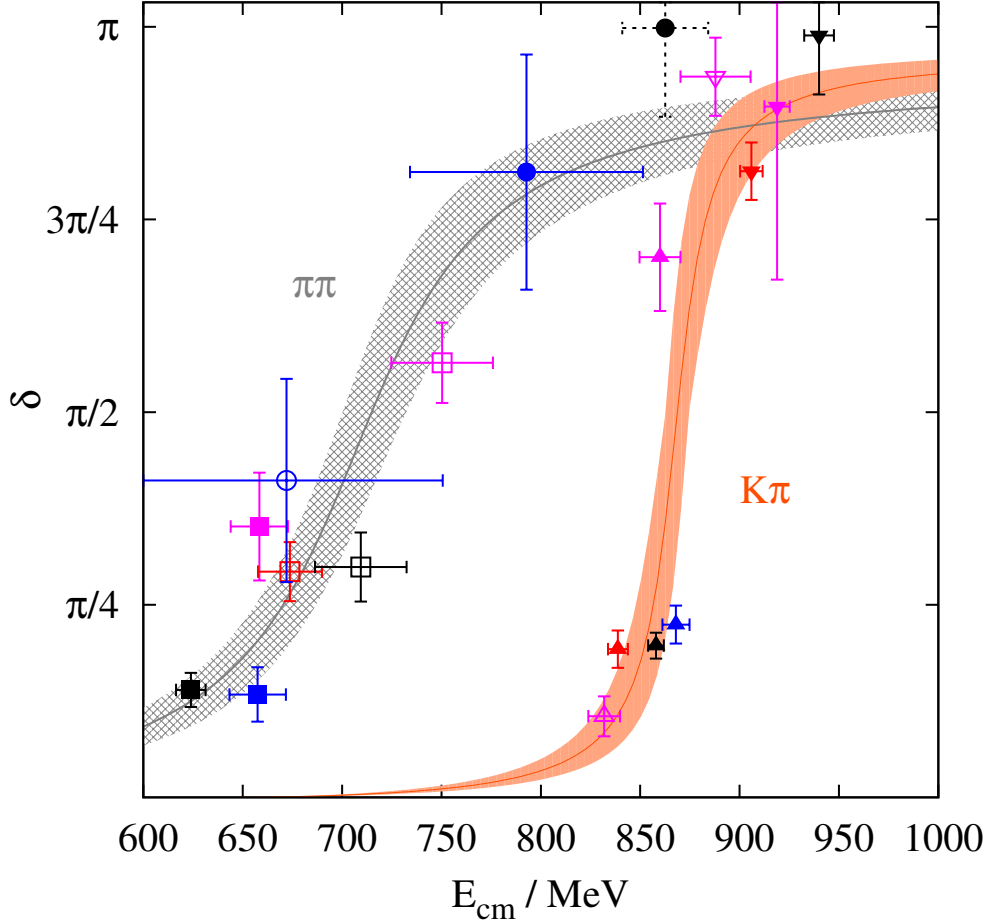
FIG. 4. The phase shift as a function of the centre of momentum frame energy, E_{cm}, for p-wave $\pi\pi$ scattering around the ρ resonance and $K\pi$ scattering around the K^* resonance. The data correspond to the lab frame energies shown in Figure 3, with matched colours and symbols. The curves with error bands are Breit-Wigner parametrizations. The dashed error bar indicates a point in $\pi\pi$ scattering which lies above the four-pion threshold.

is slightly above the respective 4π threshold. However, such decays are expected to be sub-dominant. Moreover, excluding this point from the fit only produces a hardly visible change. Since we have exact isospin symmetry, decays into three-pion final states are not possible.

Figures 3 and 4 clearly show an increase in statistical noise when going to smaller quark masses: the $\pi\pi$ scattering data have considerably larger error bars than the $K\pi$ data. From the Breit-Wigner fits shown, we find the values

$$m_\rho = 715(16)(21)\,\text{MeV}, \quad m_{K^*} = 869(6)(26)\,\text{MeV}, \tag{18}$$

$$g_{\rho\pi\pi} = 5.37 \pm 0.79, \quad g_{K^*K\pi} = 4.43 \pm 0.66, \tag{19}$$

$$\Gamma_\rho = 120(32)(4)\,\text{MeV}, \quad \Gamma_{K^*} = 26(8)(1)\,\text{MeV}, \tag{20}$$

for $\pi\pi$ and $K\pi$ scattering, where the first errors are statistical and the second errors reflect our 3% overall scale uncertainty [24]. In the last row we also quote the corre-

sponding decay widths, obtained via Eq. (16).

We emphasize that our study was carried out at a single lattice spacing only, which is not reflected in the errors given above. Both resonant masses come out smaller than the experimental values, $775\,\text{MeV}$ and $896\,\text{MeV}$, respectively. The reduced decay phase space, due to a 10% heavier than physical pion, in conjunction with somewhat smaller than physical resonance masses, is the main reason why our decay widths appear to be somewhat below the experimental ones, $\Gamma_\rho \approx 148\,\text{MeV}$ and $\Gamma_{K^*} \approx 47\,\text{MeV}$, although this difference is only statistically significant for the K^*. The coupling $g_{\rho\pi\pi}$ is consistent with the experimental value $g_{\rho\pi\pi} \approx 5.93$ while our $g_{K^*K\pi}$ is slightly lower than $g_{K^*K\pi} \approx 5.39$. The ordering $g_{\rho\pi\pi} > g_{K^*K\pi}$ is reproduced, albeit within large errors.

In Figure 5 the $\pi\pi$ phase shift curve fitted to our data is compared to the same curve with the π and ρ masses set to their physical values [26], but the coupling $g_{\rho\pi\pi}$ taken from our fit Eq. (19). As the resonant mass is
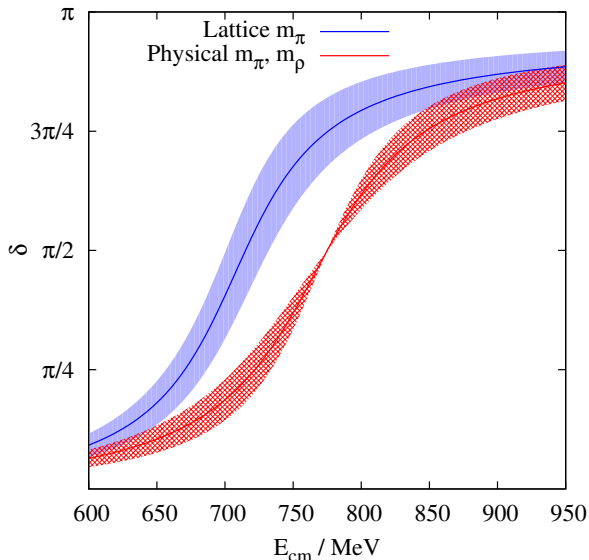
FIG. 5. We compare phase shift curves for $\pi\pi$ scattering around the ρ resonance for our fitted Breit-Wigner resonance (solid blue band) and one with the fitted coupling but physical pion and ρ masses (hashed red band).

fixed, the latter curve is forced to run through $\delta = \pi/2$ at $E_{cm} = 775\,\mathrm{MeV}$. Since our value of $g_{\rho\pi\pi}$ agrees with experiment, experimental data will be described by the hashed red band. Again, there is an overall scale setting uncertainty of 3% on E_{cm}, corresponding to 20 MeV, that we do not display as well as other systematics, most notably a 10% heavier than physical pion and a fixed lattice spacing. The figure illustrates that also in terms of the width of the resonance we are close to the physical case. Previous studies of $\pi\pi$ scattering have not directly addressed the physical limit, although unitarized chiral perturbation theory has been used in Ref. [43] to extrapolate lattice data obtained at $m_\pi \approx 236\,\mathrm{MeV}$ [18] to the physical point.

C. Impact of the finite volume pion mass shift

The pion mass enters the generalized zeta function, Eq. (14), via the calculation of the momentum carried by the two particles in the centre of momentum frame, given by Eq. (13). We prefer to use the infinite volume pion and kaon masses throughout because we are relating the spectra to scattering amplitudes in an infinite volume. For the larger $L = 64a$ lattice size, the pion mass determined in the finite volume and that extrapolated to infinite volume differ by as little as 0.2 MeV [25]. However, the pion mass measured on the $L = 48a$ configurations differs from the infinite volume mass by 10 MeV and the kaon mass by 3 MeV. Since pion exchanges around boundaries of the periodic box go beyond the Lüscher formalism, we have repeated the analysis using

finite volume pion masses instead, to explore these systematics. For the $L = 64a$ data the effect obviously is insignificant. For $L = 48a$ the phase shifts for the corresponding six points (four for the ρ resonance and two for K^*) depicted in Figure 4 (open symbols) increase by values ranging from 0.03 to 0.05. These differences are considerably smaller than our errors on δ. Indeed, using these numbers instead, we find the ρ and K^* resonance parameters $m_\rho = 712(15)\,\mathrm{MeV}$, $m_{K^*} = 868(6)\,\mathrm{MeV}$, $g_{\rho\pi\pi} = 5.29(75)$ and $g_{K^*K\pi} = 4.44(71)$, in almost perfect agreement with our main analysis employing the infinite volume pion mass Eqs. (18) and (19). For instance, the central values for the masses deviate by only $-3\,\mathrm{MeV}$ and $-1\,\mathrm{MeV}$, respectively. Adding these systematics to the statistical errors in quadrature has no impact.

Finally, in our determination of the $\pi\pi$ energy levels, we noted that there is one data point above the four-pion threshold. Excluding this from our Breit-Wigner fit, however, also had no impact worthy of mentioning.

D. Investigation of an alternative method

It is possible to estimate the value of the coupling $g_{\rho\pi\pi}$ directly from the correlators, using the McNeile-Michael-Pennanen (MMP) method introduced in Refs. [44, 45] (also see Refs. [46, 47] for earlier, related work), if the momentum and volume are selected such that the $\pi\pi$ energy is close to the resonant mass $m_\rho = m_R$. This method was also employed recently for studying the Δ resonance [48].

Using the correlators defined in Eq. (8), with $\mathcal{O}_1$ and $\mathcal{O}_2$ being two- and one-particle interpolators, we can extract (approximate) ground state energies $E_{\pi\pi}$ and E_ρ from $C_{11}(t)$ and $C_{22}(t)$ alone, respectively, at times sufficiently small to avoid the higher level to decay into the lower level (if $E_\rho \neq E_{\pi\pi}$) and large enough for excited state contributions to be negligible. In this situation, the ground state contribution to $C_{12}(t)$ reads

$$C_{12}(t) \approx xa \sum_{t'} \frac{Z_{\pi\pi}^1 Z_\rho^{2*}}{2\sqrt{E_{\pi\pi} E_\rho}} e^{-E_{\pi\pi}(t-t')} e^{-E_\rho t'}, \qquad (21)$$

where Z_α^i are the amplitudes to create the states $|\alpha\rangle$ using $\hat{\mathcal{O}}_i^\dagger$. These overlap factors also appear within $C_{11}(t)$ and $C_{22}(t)$ [see Eq. (9)] and will cancel as we are going to divide C_{12} by an appropriate combination of these two elements in Eqs. (23) and (24) below. The ρ state created at $t = 0$ will propagate to a time $t' < t$, where it undergoes a transition into $\pi\pi$. x is the associated $\rho \to \pi\pi$ transition amplitude and in Eq. (21) we summed over all possible intermediate times t'. The underlying assumption is that the overlaps of $\hat{\mathcal{O}}_2^\dagger|0\rangle$ with $|\pi\pi\rangle$ and of $\hat{\mathcal{O}}_1^\dagger|0\rangle$ with $|\rho\rangle$ are small and can be treated as perturbations, at least if t is not taken too large. Obviously, there are corrections of higher order in x to Eq. (21).

The coupling $g_{\rho\pi\pi}$ can then be estimated from x

TABLE III. Estimates of x and $g_{\rho\pi\pi}$ using the MMP method [44, 45]. The entries are sorted in terms of a descending gap $\Delta E = E_{\pi\pi} - E_\rho$. In the last row we show our result Eq. (19) from the Lüscher-type scattering analysis for comparison.

N_s	$\mathbf{K}$	Irrep	ΔE/MeV	x/MeV	$g_{\rho\pi\pi}$
48	$(0,1,1)$	A_1	135	81(5)	5.54(30)
48	$(0,1,1)$	B_1	95	106(7)	7.07(44)
48	$(0,0,1)$	E	16	124(6)	8.37(39)
48	$(0,0,0)$	T_1	-35	113(4)	7.54(28)
64	$(0,1,1)$	A_1	-122	51(2)	5.19(17)
64	$(0,1,1)$	B_1	-140	73(3)	8.18(22)
64	$(0,0,1)$	E	-173	81(2)	7.46(25)
Full scattering analysis			—	—	5.37(79)

through [45]

$$g_{\rho\pi\pi}^2 \approx \frac{L^3 E_{cm}^3}{4 p_{cm}^2} |x|^2 . \qquad (22)$$

This can be seen as follows [45]. Fermi's Golden Rule relates the decay width to the matrix element x in the centre of momentum frame: $\Gamma \approx |x|^2 L^3 p_{cm} E_{cm}/(24\pi)$. This can be re-expressed in terms of g^2 through $\Gamma = g^2 p_{cm}^3/(6\pi E_{cm}^2)$, see Eq. (16), where E_{cm} is taken at the resonance point $\delta = \pi/2$. The prefactor $L^3 p_{cm} E_{cm}/(24\pi)$ above contains the following contributions: 2π from the Golden Rule, $L^3 p_{cm} E_{cm}/(8\pi^2)$ from the density of states, $1/2$ for a decay into identical pions and $1/3$, averaging over one pion momentum direction for the fixed ρ polarization and momentum.

In Eq. (22) several assumptions have been made: (1) The Golden Rule is applicable, i.e. the $\pi\pi$ contribution to the initial ρ meson state is insubstantial and the matrix element is not too large: $|x|t \ll 1$. This is synonymous with neglecting terms of higher order in x. (2) The volumes are sufficiently large for continuous density of states methods to be applicable. (3) The $\pi\pi$ and ρ states have a similar energy and, in the centre of momentum frame, this is close to the resonant mass. (4) x does not change substantially when transforming it from the lab to the centre of momentum frame.

In the limit $E_{\pi\pi} = E_\rho$, summing over the intermediate time t', the ground state contribution to Eq. (21) has the time dependence $t\, e^{-E_{\pi\pi}t}$, while excited states are suppressed by a power of t, relative to this. In this case, x can be found from a ratio of correlators as

$$\frac{|C_{12}(t)|}{\sqrt{C_{11}(t) C_{22}(t)}} \approx \text{const.} + xt , \qquad (23)$$

up to exponential corrections in t that contribute at small times and neglecting higher powers of xt. Since only $|x|^2$ is relevant, above we defined x as real and positive. When the difference $\Delta E = E_{\pi\pi} - E_\rho$ is non-zero, we can still perform the sum over t' in Eq. (21). In this case
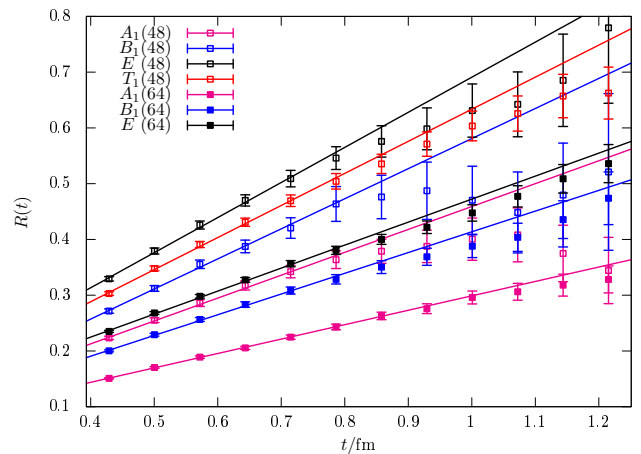

FIG. 6. The ratio of correlators $R(t)$ defined in Eq. (24) for different irreps on the two volumes, see Table III, together with linear fits to the first seven data points shown.

the time dependence of the ground state contribution is $a[\sinh(\Delta E t/2)/\sinh(\Delta E a/2)]e^{-\bar{E}t}$ (see, e.g., Ref. [48]), where the average energy is defined as $\bar{E} = \frac{1}{2}(E_{\pi\pi} + E_\rho)$. The ground state contribution of the ratio of correlators can again be used to extract x:

$$R(t) \equiv \frac{|C_{12}(t)|}{\sqrt{C_{11}(t) C_{22}(t)}} \frac{t \sinh(\Delta E\, a/2)}{a \sinh(\Delta E\, t/2)} \approx \text{const.} + xt ,$$

$$(24)$$

where we estimate ΔE from the exponential decay of the ratio $C_{11}(t)/C_{22}(t)$ at large (but not too large) times.

We now proceed to estimate $g_{\rho\pi\pi}$ to assess the reliability of the MMP method. In Figure 6 we show the resulting ratios $R(t)$, together with linear fits to the first seven data points, $6a \leq t \leq 12a$. The colour coding of the symbols corresponds to that of Figure 3. The extracted slopes scatter from 51 MeV to 124 MeV with the smaller slopes corresponding to the larger volume (full symbols), as one would expect from the naive scaling with $L^{-3/2}$ of the amplitude x defined in Eq. (21). This scaling is also consistent with Eq. (22), where the combination $x^2 L^3$ appears. For the largest slope $x \approx 124$ MeV and $t = 12a \approx 0.86$ fm, we obtain $xt \approx 0.54$. Indeed, around this Euclidean time higher order corrections in xt become relevant, while for the large volume data sets, where the slopes are smaller, the linear behaviour persists for much longer. We see no indication of exponential corrections towards small times.

In Table III we show the results for x and the derived couplings, where the errors are purely statistical. More details on the momenta and interpolators used can be found in Table II. The entries of Table III are ordered in terms of decreasing ΔE, where we find that a smaller ΔE corresponds to a smaller E_{cm} (and a smaller phase shift δ), see Figure 4. Naively, the T_1 and E irreps on the $N_s = 48$ lattice should give the most reliable results as these are closest to the resonance and best matched in terms of a small ΔE. However, only the val-

ues from the A_1 irreps are in agreement with the result from our Lüscher-type scattering analysis. We remark that in terms of the kinematics the B_1 irrep is similar to A_1, except for the orientation of the ρ spin relative to the lattice momentum $\mathbf{K} = (0, 1, 1)$. These pairs of irreps are also close to each other in terms of their ΔE values. Nevertheless, the results from the B_1 irrep differ substantially from the expectation.

Using the Lüscher method [1] has the advantage that we can directly determine the phase shift, without relying on a Breit-Wigner parametrization or introducing an effective coupling $g_{\rho\pi\pi}$. Moreover, the systematics can be controlled, while the MMP method [44, 45] relies on several approximations that cannot be tested easily. However, the statistical errors are smaller using the MMP method than in our full fledged scattering analysis. In principle we did not even have to evaluate the box diagram in the upper row of Figure 1 as formally this is of order x^2, beyond the first order perturbative ansatz. While it is encouraging that the couplings obtained are of sizes similar to the correct result, they scatter substantially between volumes and representations. Therefore, we have to assume a systematic uncertainty of the MMP method for ρ decay on our volumes of about 50%, in terms of the coupling $g_{\rho\pi\pi}$.

E. Comparison to previous results

In Figure 7, we compare our results on the ρ meson mass, extracted from the phase shift position $\delta = \pi/2$, to various literature results [6, 11, 13–19]. In Refs. [49, 50] next-to-leading order (NLO) and next-to-next-to-leading order (NNLO) chiral perturbation theory, combined with the inverse amplitude method, are used to predict the pion mass dependence of m_ρ. The quality of the available lattice data does not yet allow for a detailed comparison. The general trend seen in the majority of lattice calculations qualitatively agrees with the leading order chiral perturbation theory relation $m_\rho \propto m_\pi^2$, however, there are notable outliers.

In Figure 8 we show the coupling $g_{\rho\pi\pi}$, obtained in Refs. [6, 11–19]. Up to $m_\pi \approx 400\,\text{MeV}$, Ref. [50] expects the coupling $g_{\rho\pi\pi}$ to decrease (increase) by about 5% at NLO (NNLO), as a function of the pion mass, i.e., within the accuracy of their approach, $g_{\rho\pi\pi}$ is constant and the reduction of the decay width is purely due to phase space. An almost constant behaviour is also suggested by the KSRF relation [51, 52], $g_{\rho\pi\pi} \approx m_\rho/f_\pi \approx 5.96$, where $f_\pi = \sqrt{2}F_\pi \approx 130\,\text{MeV}$ at the physical point. In Figure 8, indeed, the lattice values up to $m_\pi \approx 470\,\text{MeV}$ are all around this coupling (which is indistinguishable from the physical coupling $g_{\rho\pi\pi} \approx 5.93$, also shown in the figure). However, the noise increases significantly, closer to the physical pion mass, so $g_{\rho\pi\pi}$ can be extracted much more accurately at large quark masses. Note that the lattice results were obtained at different lattice spacings with different actions and have quite different systemat-
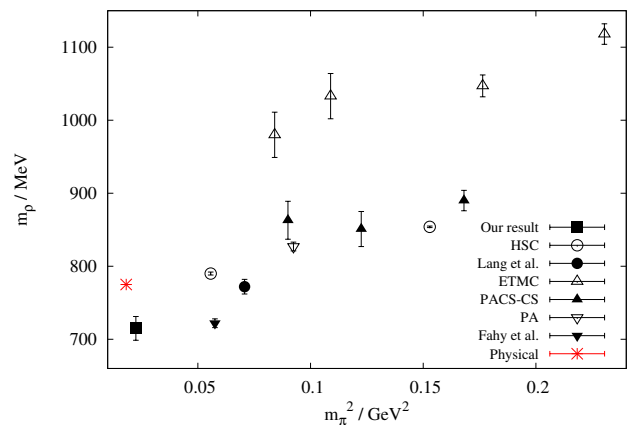

FIG. 7. ρ resonance masses from this (left most black square) and previous lattice calculations by the Hadron Spectrum Collaboration (HSC) [16, 18], Lang et al. [13], ETMC [6], PACS-CS [11, 14], Pelassier and Alexandru (PA) [15] and Fahy et al. [17, 19]. The physical value is also plotted [26]. Like the other studies, we only display our statistical error.
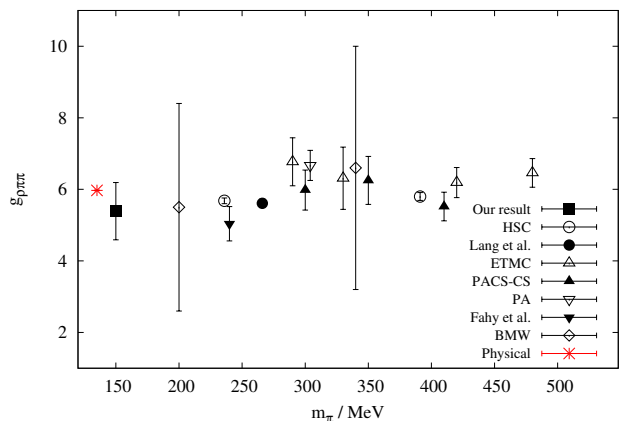

FIG. 8. Breit-Wigner couplings from various lattice calculations (Hadron Spectrum Collaboration (HSC) [16, 18], Lang et al. [13], ETMC [6], PACS-CS [11, 14], Pelassier and Alexandru (PA) [15], Fahy et al. [17] and BMW-c [12]) and that extracted from the experimentally measured ρ meson width [26].

ics.

For $K\pi$ scattering only few previous lattice studies exist. At $m_\pi \approx 150\,\text{MeV}$ and at our lattice spacing, we find $m_{K^*} = 869(6)(26)\,\text{MeV}$ and $g_{K^*\pi\pi} = 4.43(66)$. Note that in experiment $m_{K^*} \approx 896\,\text{MeV}$ and $g_{K^*K\pi} \approx 5.39$. The Hadron Spectrum Collaboration [23] reports $m_{K^*} = 933(1)\,\text{MeV}$ and $g_{K^*K\pi} = 5.72(52)$ at a pion mass of 391 MeV. Prelovšek et al. [21] use $m_\pi = 266\,\text{MeV}$ and obtain $m_{K^*} = 891(14)\,\text{MeV}$ and $g_{K^*K\pi} = 5.7(1.6)$ while Fu and Fu [20] find $m_{K^*} = 1014(27)\,\text{MeV}$ and $g_{K^*\pi\pi} = 6.38(78)$, using a lattice spacing of 0.15 fm and a pion mass of 240 MeV.

IV. CONCLUSIONS

In summary, we have demonstrated the feasibility of computing resonance scattering parameters at a nearly physical pion mass. In particular, we computed the p-wave scattering phase shifts for $\pi\pi$ scattering in the $I = 1$ channel and $K\pi$ in the $I = 1/2$ channel. From these, we extracted the masses and couplings $m_\rho = 715(16)(21)$ MeV, $\Gamma_\rho = 120(32)(4)$ MeV, $m_{K^*} = 869(6)(26)$ MeV and $\Gamma_{K^*} = 26(8)(1)$ MeV. The masses are lower than the experimental ones, $m_\rho \approx 775$ MeV, $m_{K^*} \approx 896$ MeV, and at least the width of the K^* meson is underestimated too, in part due to a 10% heavier than physical pion. The values from experiment are: $\Gamma_\rho \approx 148$ MeV, $\Gamma_{K^*} \approx 47$ MeV [26]. The second errors reflect an overall scale uncertainty of 3% [24]. While for the ρ meson mass and width this error can be added in quadrature to the statistical one, for the K^* parameters it is not straightforward to account for this uncertainty as our strange quark mass was tuned, assuming $a^{-1} = 2.76$ GeV.

The stochastic one-end source method we have used is cheaper compared to other methods [17, 53, 54], as long as the set of kinematic points (and interpolators) is suitably restricted. In our calculation, we were able to recycle many propagators, by keeping one of the momenta, $\mathbf{p}_1$, fixed. The number of inversions required is given in Eq. (7) and the cost of including additional momenta is large. This is a limitation in particular for larger volumes, when the density of states increases and the use of multiple two-particle interpolators cannot be avoided. We remark, however, that our larger volume with a linear lattice extent $64a \approx 4.6$ fm is not at all small considering present-day standards in lattice scattering computations.

An alternative approach is the distillation method [53], which has been used in several other scattering calculations [13, 16, 18]. This method does not suffer from a large computational overhead when including additional momenta as time-slice-to-all propagators (perambulators) are used in constructing the correlators. However, this method is not very well suited to large volumes as the number of vectors required increases in proportion to $L^3 N_t$ and the cost of contractions also scales with a power of the number of vectors. Combining this method with stochastic estimates [54] may ultimately not change this scaling behaviour but may make realistic lattice sizes accessible. Indeed, this stochastic distillation method has been successfully employed for $\pi\pi$ scattering [17, 19], where the number of solves used in Ref. [19] is not much higher than ours. It will be very interesting to see if such calculations can be pushed towards small quark masses, large volumes and time distances of about 1 fm that allow for a reliable extraction of energy levels.

Stochastic distillation was also successfully used to study DK scattering [55–57].

Our calculation is performed at a single lattice spacing and it is not possible to quantify the size of discretization effects. For the action we use, these are of $\mathcal{O}(a^2)$ and it is unlikely at our lattice spacing $a \approx 0.071$ fm that they are much larger than our scale uncertainty. Limited information for the $\mathcal{O}(a^2)$ accurate twisted mass action can be extracted from the results for the ρ meson mass given in Ref. [58]. In this study of the hadronic vacuum polarization contribution to $(g-2)_\mu$, the correlators for vector mesons are calculated only using a one-particle interpolator for several ensembles with different lattice spacings and (larger than physical) pion masses. The mass of the ρ is then found by treating it as a stable particle and the results obtained show no significant dependence on the lattice spacing. We therefore assume that the 3% scale uncertainty and the 10% larger than physical pion mass are our dominant systematics.

In Figures 7 and 8 we compare our results on the ρ meson mass and coupling to those of other lattice studies that were carried out at larger pion masses. The coupling $g_{\rho\pi\pi}$ appears to be remarkably independent of the quark mass.

Future work will extend the present study to $N_f = 2+1$ flavour configurations, including several lattice spacings, to enable a continuum limit extrapolation. Working close to the physical pion mass is particularly valuable for simulations of scattering processes involving states that are near to thresholds, e.g., $X(3872)$ and $D\overline{D}^*$ or $D_{s0}(2317)$ and DK, where the gap relative to the threshold strongly depends on the light quark mass.

[1] Martin Lüscher, "Two particle states on a torus and their relation to the scattering matrix," Nucl. Phys. **B354**, 531 (1991).

[2] Martin Lüscher, "Volume dependence of the energy spectrum in massive quantum field theories. 2. Scattering states," Commun. Math. Phys. **105**, 153 (1986).

[3] Kari Rummukainen and Steven A. Gottlieb, "Resonance scattering phase shifts on a nonrest frame lattice," Nucl. Phys. **B450**, 397 (1995), arXiv:hep-lat/9503028 [hep-lat].

[4] Changhoan Kim, Christopher T. Sachrajda, and Stephen R. Sharpe, "Finite-volume effects for two-hadron states in moving frames," Nucl. Phys. **B727**, 218 (2005), arXiv:hep-lat/0507006 [hep-lat].

[5] Norman H. Christ, Changhoan Kim, and Takeshi Yamazaki, "Finite volume corrections to the two-particle decay of states with non-zero momentum," Phys. Rev. D **72**, 114506 (2005), arXiv:hep-lat/0507009 [hep-lat].

[6] Xu Feng, Karl Jansen, and Dru B. Renner, "Resonance parameters of the ρ-meson from lattice QCD," Phys. Rev. D **83**, 094505 (2011), arXiv:1011.5288 [hep-lat].

[7] Zohreh Davoudi and Martin J. Savage, "Improving the volume dependence of two-body binding energies calculated with lattice QCD," Phys. Rev. D **84**, 114502 (2011), arXiv:1108.5371 [hep-lat].

[8] Ziwen Fu, "Rummukainen-Gottlieb's formula on two-particle system with different mass," Phys. Rev. D **85**, 014506 (2012), arXiv:1110.0319 [hep-lat].

[9] Luka Leskovec and Saša Prelovšek, "Scattering phase shifts for two particles of different mass and non-zero total momentum in lattice QCD," Phys. Rev. D **85**, 114507 (2012), arXiv:1202.2145 [hep-lat].

[10] M. Göckeler, R. Horsley, M. Lage, U.-G. Meißner, P. E. L. Rakow, A. Rusetsky, G. Schierholz, and J. M. Zanotti, "Scattering phases for meson and baryon resonances on general moving-frame lattices," Phys. Rev. D **86**, 094513 (2012), arXiv:1206.4141 [hep-lat].

[11] Sinya Aoki *et al.* (CP-PACS Collaboration), "Lattice QCD calculation of the rho meson decay width," Phys. Rev. D **76**, 094506 (2007), arXiv:0708.3705 [hep-lat].

[12] J. Frison *et al.* (BMW-c), "Rho decay width from the lattice," *Proceedings, 28th International Symposium on Lattice field theory (Lattice 2010)*, Proc. of Science **LATTICE2010**, 139 (2010), arXiv:1011.3413 [hep-lat].

[13] C. B. Lang, Daniel Mohler, Saša Prelovšek, and Matija Vidmar, "Coupled channel analysis of the rho meson decay in lattice QCD," Phys. Rev. D **84**, 054503 (2011), [Erratum: Phys. Rev. D 89 (2014) 059903(E)], arXiv:1105.5636 [hep-lat].

[14] Sinya Aoki *et al.* (PACS-CS Collaboration), "ρ meson decay in 2+1 flavor lattice QCD," Phys. Rev. D **84**, 094505 (2011), arXiv:1106.5365 [hep-lat].

[15] Craig Pelissier and Andrei Alexandru, "Resonance parameters of the rho-meson from asymmetrical lattices," Phys. Rev. D **87**, 014503 (2013), arXiv:1211.0092 [hep-lat].

[16] Jozef J. Dudek, Robert G. Edwards, and Christopher E. Thomas (Hadron Spectrum Collaboration), "Energy dependence of the ρ resonance in $\pi\pi$ elastic scattering from lattice QCD," Phys. Rev. D **87**, 034505 (2013), [Erratum: Phys. Rev.D90 (2014) 099902(E)], arXiv:1212.0830 [hep-ph].

[17] Brendan Fahy, John Bulava, Ben Hörz, Keisuke J. Juge, Colin Morningstar, and Chik Him Wong, "Pion-pion scattering phase shifts with the stochastic LapH method," *Proceedings, 32nd International Symposium on Lattice Field Theory (Lattice 2014)*, Proc. of Science **LATTICE2014**, 077 (2015), arXiv:1410.8843 [hep-lat].

[18] David J. Wilson, Raúl A. Briceño, Jozef J. Dudek, Robert G. Edwards, and Christopher E. Thomas, "Coupled $\pi\pi, K\overline{K}$ scattering in P-wave and the ρ resonance from lattice QCD," Phys. Rev. D **92**, 094502 (2015), arXiv:1507.02599 [hep-ph].

[19] John Bulava, Ben Hörz, Brendan Fahy, K. J. Juge, Colin Morningstar, and Chik Him Wong, "Pion-pion scattering and the timelike pion form factor from $N_{\mathrm{f}} = 2 + 1$ lattice QCD simulations using the stochastic LapH method," in *Proceedings, 33rd International Symposium on Lattice Field Theory (Lattice 2015)* (2015) arXiv:1511.02351 [hep-lat].

[20] Ziwen Fu and Kan Fu, "Lattice QCD study on $K^*(892)$ meson decay width," Phys. Rev. 86 **86**, 094507 (2012), arXiv:1209.0350 [hep-lat].

[21] Saša Prelovšek, Luka Leskovec, C. B. Lang, and Daniel Mohler, "K π scattering and the K^* decay width from lattice QCD," Phys. Rev. D **88**, 054508 (2013), arXiv:1307.0736 [hep-lat].

[22] Jozef J. Dudek, Robert G. Edwards, Christopher E. Thomas, and David J. Wilson (Hadron Spectrum Collaboration), "Resonances in coupled $\pi K - \eta K$ scattering from quantum chromodynamics," Phys. Rev. Lett. **113**, 182001 (2014), arXiv:1406.4158 [hep-ph].

[23] David J. Wilson, Jozef J. Dudek, Robert G. Edwards, and Christopher E. Thomas, "Resonances in coupled $\pi K, \eta K$ scattering from lattice QCD," Phys. Rev. D **91**, 054008 (2015), arXiv:1411.2004 [hep-ph].

[24] Gunnar S. Bali *et al.* (QCDSF Collaboration), "Nucleon mass and sigma term from lattice QCD with two light fermion flavors," Nucl. Phys. **B866**, 1 (2013), arXiv:1206.7034 [hep-lat].

[25] Gunnar S. Bali, Sara Collins, Benjamin Gläßle, Meinulf Göckeler, Johannes Najjar, Rudolf H. Rödl, Andreas Schäfer, Rainer W. Schiel, André Sternbeck, and Wolfgang Söldner, "The moment $\langle x \rangle_{u-d}$ of the nucleon from $N_f = 2$ lattice QCD down to nearly physical quark masses," Phys. Rev. D **90**, 074510 (2014), arXiv:1408.6850 [hep-lat].

[26] Keith A. Olive *et al.* (Particle Data Group), "Review of Particle Physics," Chin. Phys. **C38**, 090001 (2014).

[27] R. R. Akhmetshin *et al.* (CMD-2), "Cross-section of the reaction $e^+e^- \rightarrow \pi^+\pi^-\pi^+\pi^-$ below 1 GeV at CMD-2," Phys. Lett. **B475**, 190 (2000), arXiv:hep-ex/9912020 [hep-ex].

[28] M. N. Achasov *et al.*, "Study of the process $e^+e^- \rightarrow \pi^+\pi^-\pi^0$ in the energy region $\sqrt{s}$ below 0.98 GeV," Phys. Rev. D **68**, 052006 (2003), arXiv:hep-ex/0305049 [hep-ex].

[29] B. Jongejans *et al.* (Amsterdam-CERN-Nijmegen-Oxford Collaboration), "Rare decay modes of $K^*(1420)$ and $K^*(892)$," Nucl. Phys. **B139**, 383 (1978).

[30] D. Aston *et al.*, "The strange meson resonances observed in the reaction $K^-p \rightarrow \overline{K}^0\pi^+\pi^-n$ at 11 GeV/c," Nucl. Phys. **B292**, 693 (1987).

[31] Gunnar S. Bali, Sara Collins, Benjamin Glässle, Meinulf Göckeler, Johannes Najjar, Rudolf H. Rödl, Andreas Schäfer, Rainer W. Schiel, Wolfgang Söldner, and André Sternbeck, "Nucleon isovector couplings from $N_f = 2$ lattice QCD," Phys. Rev. D **91**, 054501 (2015), arXiv:1412.7336 [hep-lat].

[32] Gunnar S. Bali *et al.* (QCDSF Collaboration), "The strange and light quark contributions to the nucleon mass

from lattice QCD," Phys. Rev. D **85**, 054502 (2012), arXiv:1111.1600 [hep-lat].

[33] M. Albaladejo, G. Rios, J. A. Oller, and L. Roca, "Finite volume treatment of $\pi\pi$ scattering in the ρ channel," (2013), arXiv:1307.5169 [hep-lat].

[34] Maxwell T. Hansen and Stephen R. Sharpe, "Relativistic, model-independent, three-particle quantization condition," Phys. Rev. D **90**, 116003 (2014), arXiv:1408.5933 [hep-lat].

[35] Ulf-G. Meißner, Guillermo Ríos, and Akaki Rusetsky, "Spectrum of three-body bound states in a finite volume," Phys. Rev. Lett. **114**, 091602 (2015), arXiv:1412.4969 [hep-lat].

[36] Maxwell T. Hansen and Stephen R. Sharpe, "Expressing the three-particle finite-volume spectrum in terms of the three-to-three scattering amplitude," Phys. Rev. D **92**, 114509 (2015), arXiv:1504.04248 [hep-lat].

[37] Stefan Güsken, Ute Löw, Karl Heinz Mütter, Rainer Sommer, Apoorva Patel, and Klaus Schilling, "Nonsinglet axial vector couplings of the baryon octet in lattice QCD," Phys. Lett. **B227**, 266 (1989).

[38] Massimo Falcioni, Maria Luigia Paciello, Giorgio Parisi, and Bruno Taglienti (APE Collaboration), "Again on SU(3) glueball mass," Nucl. Phys. **B251**, 624 (1985).

[39] Morton Hamermesh, *Group theory and its application to physical problems* (Addison-Wesley, Reading, MA, 1962).

[40] Christopher Michael, "Adjoint sources in Lattice Gauge Theory," Nucl. Phys. **B259**, 58 (1985).

[41] Martin Lüscher and Ulli Wolff, "How to calculate the elastic scattering matrix in two-dimensional Quantum Field Theories by numerical simulation," Nucl. Phys. **B339**, 222 (1990).

[42] Benoit Blossier, Michele Della Morte, Georg von Hippel, Tereza Mendes, and Rainer Sommer, "On the generalized eigenvalue method for energies and matrix elements in lattice field theory," JHEP **04**, 094 (2009), arXiv:0902.1265 [hep-lat].

[43] Daniel R. Bolton, Raúl A. Briceño, and David J. Wilson, "Connecting physical resonant amplitudes and lattice QCD," (2015), arXiv:1507.07928 [hep-ph].

[44] Craig McNeile, Christopher Michael, and Petrus Pennanen (UKQCD Collaboration), "Hybrid meson decay from the lattice," Phys. Rev. D **65**, 094505 (2002), arXiv:hep-lat/0201006 [hep-lat].

[45] Craig McNeile and Christopher Michael (UKQCD Collaboration), "Hadronic decay of a vector meson from the lattice," Phys. Lett. **B556**, 177 (2003), arXiv:hep-lat/0212020 [hep-lat].

[46] Steven A. Gottlieb, Paul B. Mackenzie, Hank B. Thacker, and Don Weingarten, "The ρ-$\pi\pi$ coupling constant in lattice gauge theory," Phys. Lett. **B134**, 346 (1984).

[47] Steven A. Gottlieb, Paul B. MacKenzie, Hank B. Thacker, and Don Weingarten, "Hadronic couplings constants in Lattice Gauge Theory," Nucl. Phys. **B263**, 704 (1986).

[48] C. Alexandrou, J. W. Negele, M. Petschlies, A. Strelchenko, and A. Tsapalis, "Determination of Δ resonance parameters from lattice QCD," Phys. Rev. D **88**, 031501 (2013), arXiv:1305.6081 [hep-lat].

[49] C. Hanhart, J. R. Peláez, and G. Rios, "Quark mass dependence of the rho and sigma from dispersion relations and Chiral Perturbation Theory," Phys. Rev. Lett. **100**, 152001 (2008), arXiv:0801.2871 [hep-ph].

[50] José R. Peláez and Guillermo Rios, "Chiral extrapolation of light resonances from one and two-loop unitarized Chiral Perturbation Theory versus lattice results," Phys. Rev. D **82**, 114002 (2010), arXiv:1010.6008 [hep-ph].

[51] Ken Kawarabayashi and Mahiko Suzuki, "Partially conserved axial vector current and the decays of vector mesons," Phys. Rev. Lett. **16**, 255 (1966).

[52] Riazuddin and Fayyazuddin, "Algebra of current components and decay widths of rho and K^* mesons," Phys. Rev. **147**, 1071 (1966).

[53] Michael Peardon, John Bulava, Justin Foley, Colin Morningstar, Jozef Dudek, Robert G. Edwards, Balint Joó, Huey-Wen Lin, David G. Richards, and Keisuke Jimmy Juge (Hadron Spectrum Collaboration), "A Novel quark-field creation operator construction for hadronic physics in lattice QCD," Phys. Rev. D **80**, 054506 (2009), arXiv:0905.2160 [hep-lat].

[54] Colin Morningstar, John Bulava, Justin Foley, Keisuke J. Juge, David Lenkner, Mike Peardon, and Chik Him Wong, "Improved stochastic estimation of quark propagation with Laplacian Heaviside smearing in lattice QCD," Phys. Rev. D **83**, 114505 (2011), arXiv:1104.3870 [hep-lat].

[55] Daniel Mohler, C. B. Lang, Luka Leskovec, Saša Prelovšek, and Richard M. Woloshyn, "$D_{s0}^*(2317)$ meson and D-meson-kaon scattering from lattice QCD," Phys. Rev. Lett. **111**, 222001 (2013), arXiv:1308.3175 [hep-lat].

[56] C. B. Lang, Luka Leskovec, Daniel Mohler, Saša Prelovšek, and Richard M. Woloshyn, "D_s mesons with DK and D^*K scattering near threshold," Phys. Rev. D **90**, 034510 (2014), arXiv:1403.8103 [hep-lat].

[57] C. B. Lang, Daniel Mohler, Saša Prelovšek, and Richard M. Woloshyn, "Predicting positive parity B$_s$ mesons from lattice QCD," Phys. Lett. **B750**, 17 (2015), arXiv:1501.01646 [hep-lat].

[58] Florian Burger, Xu Feng, Grit Hotzel, Karl Jansen, Marcus Petschlies, and Dru B. Renner (ETM Collaboration), "Four-flavour leading-order hadronic contribution to the muon anomalous magnetic moment," JHEP **02**, 099 (2014), arXiv:1308.4327 [hep-lat].

[59] Robert G. Edwards and Balint Joó (SciDAC, LHPC and UKQCD Collaborations), "The Chroma software system for lattice QCD," Nucl. Phys. B Proc. Suppl. **140**, 832 (2005), arXiv:hep-lat/0409003 [hep-lat].

[60] http://luscher.web.cern.ch/luscher/openQCD/,.

[61] H. Baier *et al.*, "QPACE: A QCD parallel computer based on Cell processors," Proc. of Science **LAT2009**, 001 (2009), arXiv:0911.2174 [hep-lat].

[62] Y. Nakamura, A. Nobile, D. Pleiter, H. Simma, T. Streuer, T. Wettig, and F. Winter, "Lattice QCD applications on QPACE," Procedia Computer Science **Vol. 4**, 841 (2011), arXiv:1103.1363 [hep-lat].

[63] Yoshifumi Nakamura and Hinnerk Stüben, "BQCD - Berlin quantum chromodynamics program," *Proceedings, 28th International Symposium on Lattice field theory (Lattice 2010)*, Proc. of Science **LATTICE2010**, 040 (2010), arXiv:1011.0199 [hep-lat].

[64] Simone Gutzwiller, "Scattering phase shift for elastic two pion scattering and the rho resonance in lattice QCD," (2012).